







# NeuTracker—imaging neurobehavioral dynamics in freely behaving fish

Panagiotis Symvoulidis<sup>1–3</sup> , Antonella Lauri<sup>1–3</sup>, Anca Stefanoiu<sup>4</sup>, Michele Cappetta<sup>1–3</sup>, Steffen Schneider<sup>3</sup>, Hongbo Jia<sup>5</sup>, Anja Stelzl<sup>1,2</sup>, Maximilian Koch<sup>1</sup> , Carlos Cruz Perez<sup>1,2</sup>, Ahne Myklatun<sup>1–3</sup>, Sabine Renninger<sup>6</sup> , Andriy Chmyrov<sup>1,7</sup> , Tobias Lasser<sup>4</sup> , Wolfgang Wurst<sup>2</sup>, Vasilis Ntziachristos<sup>1,7</sup> & Gil G Westmeyer<sup>1–3</sup> 

**A long-standing objective in neuroscience has been to image distributed neuronal activity in freely behaving animals. Here we introduce NeuTracker, a tracking microscope for simultaneous imaging of neuronal activity and behavior of freely swimming fluorescent reporter fish. We showcase the value of NeuTracker for screening neurostimulants with respect to their combined neuronal and behavioral effects and for determining spontaneous and stimulus-induced spatiotemporal patterns of neuronal activation during naturalistic behavior.**

An important goal in neuroscientific research is to record spatiotemporal patterns of brain activity in freely moving animals in order to reveal neuronal correlates of unperturbed perception and unrestrained behavior. However, a combination of physical restraint, pharmacological sedation and paralysis of the animal is typically necessary to enable neuroimaging. Whereas head-mounted optical imaging devices have been developed for rodents to achieve real-time neuroimaging of selected cell populations in freely moving animals<sup>1</sup>, the accessible fields of view (FOVs) are usually much smaller than what can be achieved in transparent fish.

Advances in genetically encoded fluorescent sensors<sup>2</sup> and fast imaging instrumentation have established zebrafish (*Danio rerio*) as a powerful genetic vertebrate model organism for imaging-based neuroscience<sup>3</sup>. Virtual reality approaches in restrained zebrafish larvae<sup>4–6</sup>, fluorescent imaging of unrestrained fish within a stationary FOV<sup>7</sup>, and bioluminescent point measurements in freely behaving larvae<sup>8</sup> have been reported. There is also considerable interest in quantifying the versatile behavioral repertoire of zebrafish<sup>9,10</sup> in the context of high-throughput pharmacological screens<sup>11</sup>.

Here we introduce an open-source and modular platform for neurobehavioral interrogation (NeuTracker) that enables

simultaneous and noninvasive monitoring of brain activity and behavioral parameters in freely swimming zebrafish larvae.

Fluorescent imaging solutions for nonvertebrate organisms such as *Caenorhabditis elegans* have been developed that utilize motorized stages to keep the animal in the FOV<sup>12</sup>. However, to achieve neuroimaging of swimming zebrafish larvae, this approach would necessitate moving a water-filled arena with such acceleration that confounding mechanosensory stimulation of the animals could occur. Furthermore, compared with *Drosophila*, from whose brain fluorescent data were obtained with a conventional photographic lens after surgical removal of the head cuticle<sup>13</sup>, the transparency of zebrafish larvae affords tracking fluorescently labeled cells throughout the body, and this makes adjustable FOVs desirable. Zebrafish larvae also swim at different depths depending on their developmental stage and behavioral context.

To meet these specifications, we have built NeuTracker to (i) operate without moving stages, objectives or excitation light beams; (ii) provide adjustable magnification; and (iii) allow for dynamic refocusing (Fig. 1a,b; Supplementary Figs. 1–3; Supplementary Video 1). NeuTracker has two imaging channels—one is static to observe the behavior of the fish and locate its position, the other one tracks the freely swimming larva to provide magnified fluorescent images. Tracking of the fish is controlled by a custom-written acquisition software that receives the 1× image from an IR-sensitive camera as input, locates the fish's head, and moves galvanometric mirrors to the position that keeps the FOV of the fluorescent camera on the fish (Supplementary Fig. 4–6). A postprocessing algorithm coregisters the acquired images to enable analysis of the spatiotemporal patterns of calcium fluxes (Supplementary Figs. 4 and 7). For fluorescence excitation, we used an ~3.3-W LED centered at 460 nm to provide homogeneous illumination across the whole arena (Supplementary Fig. 3h,i) rather than guiding the excitation light through the tracking mirrors, which might result in confounding visual or thermal stimuli during imaging<sup>14,15</sup>. Magnification is obtained either by using lenses with a fixed focal length ('MicroFixed' configuration) or a zoom lens ('MacroZoom' configuration), which can achieve a resolution of up to 150 line pairs per mm (lp/mm) for FOVs ranging from the whole body of a larva to zoom-ins on only the larval brain (Fig. 1a,b and Supplementary Fig. 1). Furthermore, we inserted an electrically tunable lens (ETL) to enable fast refocusing with submicrometer steps up to a focal length of 10 mm (Supplementary Fig. 8).

NeuTracker allowed us to simultaneously image the behavior and neuronal activity of freely swimming larvae expressing fluorescent calcium indicators. In fish with strong pan-neuronal expression of GCaMP6s, we found voxel time courses in the hindbrain that were significantly correlated ( $P < 10^{-5}$ ,

<sup>1</sup>Institute of Biological and Medical Imaging, Helmholtz Zentrum München, Munich, Germany. <sup>2</sup>Institute of Developmental Genetics, Helmholtz Zentrum München, Munich, Germany. <sup>3</sup>Department of Nuclear Medicine, Technical University of Munich, Munich, Germany. <sup>4</sup>Computer Aided Medical Procedures, Technical University of Munich, Munich, Germany. <sup>5</sup>Institute of Neuroscience, Technical University of Munich, Munich, Germany. <sup>6</sup>Champalimaud Centre for the Unknown, Lisbon, Portugal. <sup>7</sup>Chair for Biological Imaging, Technical University of Munich, Munich, Germany. Correspondence should be addressed to G.G.W. (gil.westmeyer@tum.de).

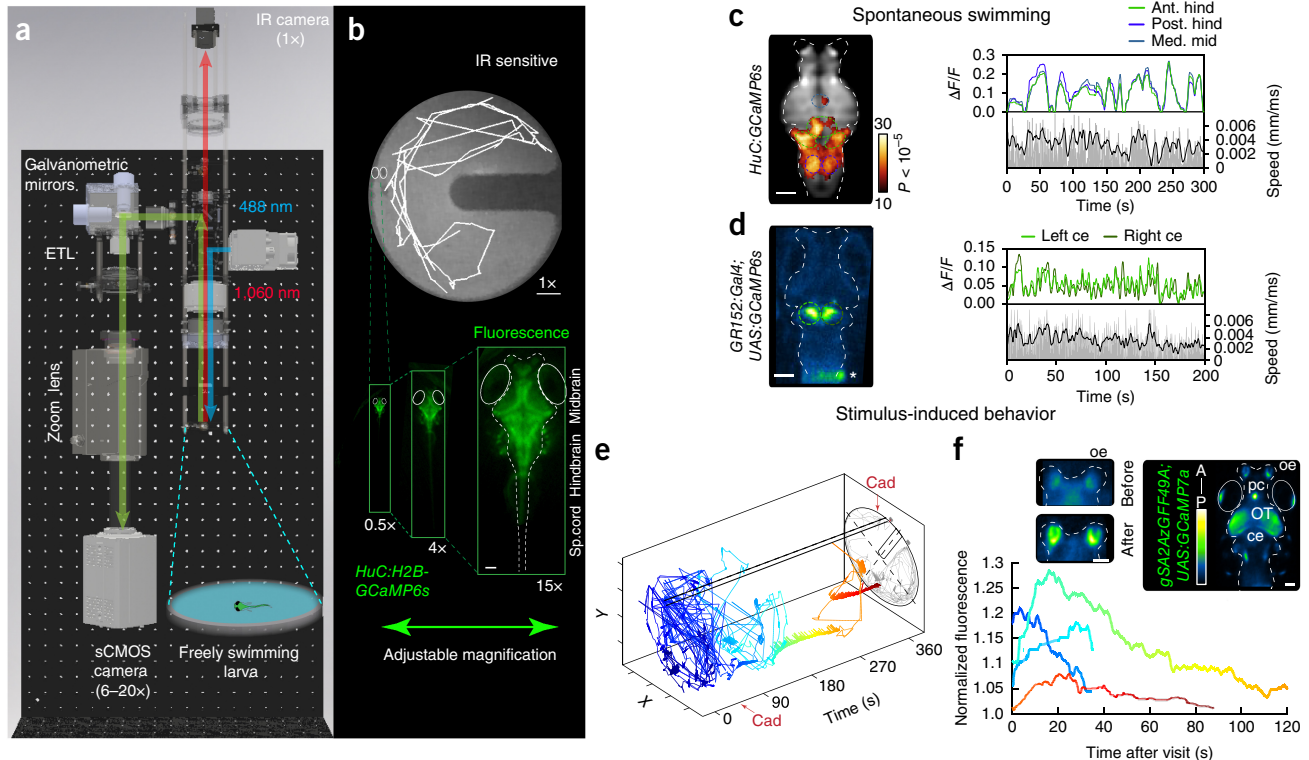


**Figure 1** | Design and performance of NeuBtracker. **(a)** Rendering of the system showing the infrared (IR) channel (red arrow) for transillumination imaging as well as the fluorescence detection path (blue/green) that can be scanned across the arena with adjustable magnification and focusing via an electrically tunable lens (ETL). **(b)** Example of a swimming trajectory as well as fluorescent images obtained at different magnifications either capturing the whole arena (0.5 $\times$ ), covering the entire body ( $\sim$ 4 $\times$ ) or just the brain ( $\sim$ 15 $\times$ ) of a larva with pan-neuronal expression of GCaMP6s (*tg(HuC:H2B-GCaMP6s)*, 7 d postfertilization (dpf)). Scale bar on the arena, 1 mm; scale bar for the fluorescent image, 100  $\mu$ m. **(c)** Neurobehavioral imaging data from a spontaneously swimming zebrafish larva with pan-neuronal expression of GCaMP6s (*tg(HuC:GCaMP6s)*). Linear regression analysis revealed areas of the anterior and posterior hindbrain (ant. and post. hind) that were correlated with the swimming speed of the larva (coefficient map thresholded at a *P* value of 0.01, Bonferroni corrected to *P* = 10 $^{-5}$ ) overlaid on the time-averaged image (displayed on grayscale). Right, corresponding fluorescent signal time courses color coded for the ROIs drawn on the map (med. mid., medial midbrain). **(d)** Fluorescent signal changes ( $\Delta F/F$ ) in the cerebellum during spontaneous swimming of a larva with GCaMP6s expression in the granule cells of the cerebellum (*tg(GR152:Gal4;UAS:GCaMP6s)*). \* denotes non-neuronal autofluorescence. **(e)** Swimming trajectory of a larva with predominant expression of GCaMP7a in the optic tectum (OT) and anterior brain regions including the olfactory epithelium (oe) (*tg(gSA2AzGFF49A;UAS:GCaMP7a)*) before and after local administration of the odorant cadaverine (Cad, red arrows) into the left compartment of the test arena. **(f)** Fluorescent signal traces (normalized to the baseline signal) in the olfactory epithelium (oe) after multiple visits to the cadaverine port (color coded for time as in **e**). The insets show zoom-ins to oe before and after addition of Cad. Scale bars, 100  $\mu$ m.

*t*-test on regression coefficient) with swimming speed during spontaneous swimming (**Fig. 1c** and **Supplementary Fig. 9a,b**; maximum correlation in the hindbrain, *R* = 0.48). This activation pattern partially overlaps with patterns observed in recent studies, in which fictive swimming was elicited in paralyzed larvae by presenting moving visual gratings<sup>5,6</sup>. Furthermore, we could detect calcium activity correlated with swimming speed in a zebrafish line with GCaMP6s expression in cerebellar granule cells (**Fig. 1d** and **Supplementary Fig. 9c**; correlation in the cerebellar region of interest (ROI), *R* = 0.45).

To analyze stimulus-induced neurobehavioral responses, we applied the odorant cadaverine<sup>16</sup> into one of two reservoirs of a custom-built arena such that it could diffuse on one side of a central divider (**Fig. 1e** and **Supplementary Fig. 10a,b**). We simultaneously tracked the swimming trajectory and the neuronal activity of larvae exhibiting prominent expression of GCaMP7a in the optic tectum and anterior brain regions<sup>7</sup> and observed repeated activations of the fish's olfactory epithelium after multiple visits to the cadaverine port (**Fig. 1e,f** and control experiments shown in **Supplementary Fig. 11**).

We then used NeuBtracker for studying neurobehavioral effects upon delivery of neuroactive compounds to complement high-throughput drug screens based only on behavioral readouts with simultaneous observation of brain activity<sup>11</sup>. We imaged two groups of *tg(HuC:GCaMP6s)* larvae stimulated with either 4-aminopyridine (4-AP) or vehicle control. The first group received 4-AP directly at 150 s from the start of the recording (*t*<sub>1</sub>), while the second group obtained water at *t*<sub>1</sub> and then 4-AP at 300 s (*t*<sub>2</sub>). In the time period after drug administration, we observed an increase in the fluorescent signal change of more than 50% in some brain regions (**Fig. 2a**). In line with this, we detected an increase in average swimming velocity and more frequent swimming bursts after application of 4-AP (**Fig. 2b**). These data demonstrate how NeuBtracker can be used to screen neuroactive drugs in neurobehavioral screening assays, the throughput of which can be increased by using motorized stages and multiwell plates (**Supplementary Fig. 10f,g**).

Next, we sought to establish long-term recordings under IR illumination with optional intermittent periods of fluorescence imaging. When we imaged zebrafish with preferential expression of

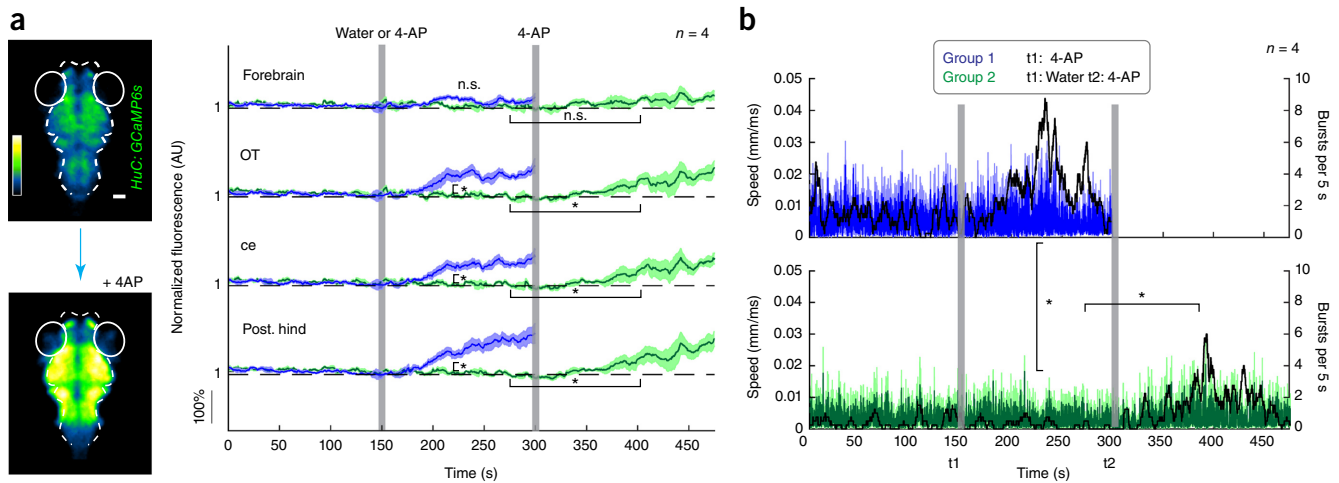


**Figure 2** | Neurobehavioral responses to the neurostimulant 4-AP. **(a)** Left, representative fluorescent images from freely swimming zebrafish larvae expressing GCaMP6s (*tg(HuC:GCaMP6s)*), 5 dpf recorded on NeuBtracker before (top) and after (bottom) stimulation with the neuroactive drug 4-aminopyridine (4-AP). Scale bars, 100  $\mu$ m. Right, fluorescent signal changes in different brain regions shown for two groups of fish (normalized to the baseline and averaged over animals, plotted with s.e.m.). After 150 s (t1), larvae in group 1 ( $n = 4$ , blue traces) were stimulated with 4-AP ( $\sim 1,200 \mu$ M) added to the water of the arena which led to a significant increase in the GCaMP6s signal in the optic tectum (OT), cerebellum (ce), posterior hindbrain (post. hind) but not forebrain as compared to a vehicle control group of larvae (group 2,  $n = 4$ , green traces) that received only fish water at t1 ( $t$ -test,  $P$  values = 0.018, 0.032, 0.046 and 0.105 for the listed ROIs, respectively, see vertical brackets). Group 2 received 4-AP ( $\sim 1,200 \mu$ M) at a later timepoint t2, which led to a significant increase of the fluorescent signal in OT, ce, and post. hind when compared to the preinjection period (paired  $t$ -test,  $P$  values = 0.03, 0.03, 0.04 for the respective ROIs; see horizontal brackets). No significant increase was observed in the forebrain (paired  $t$ -test,  $P$  value = 0.07). **(b)** The mean swimming speed (plotted with s.e.m. in lighter colors) of the two different groups (left  $y$ -axis) of fish was significantly increased compared to the vehicle control group ( $t$ -test,  $P$  value = 0.045). Group 2 also showed an increase in swimming speed after addition of 4-AP (paired  $t$ -test,  $P$  value = 0.049). The median counts of swimming bursts (instances of swimming speeds faster than 0.05 mm/ms counted over 5-s time windows) are shown as black solid lines (right  $y$ -axis).

GCaMP7a in light-responsive brain regions<sup>7</sup>, we not only found a substantial increase in locomotor activity during periods when the blue LED was off, but also captured an elevated and subsequently decaying fluorescent signal in the pineal complex (pc) when the blue LED was turned on. The fluorescent signal time courses in pc recorded by NeuBtracker from a freely swimming larva during several dark–light cycles exhibited an exponential decay when averaged over cycles (Fig. 3a) or over animals (Supplementary Fig. 12a), which was not observed in the optic tectum (OT). Behavioral analysis showed that the distance traveled was substantially different between the illumination conditions (Fig. 3b,c). We confirmed the exponential signal decay in pc in an immobilized larva using a custom-built selective plane illumination microscope (SPIM) (Fig. 3d) and verified strong expression of GCaMP within cells of pc (known to possess nonvisual photoreceptors) by two-photon microscopy (Supplementary Fig. 12b). In addition, we confirmed the activation of pc through changes in the light conditions by neuronal-activity-dependent immunohistochemistry against phosphorylated ERK<sup>17</sup> (Supplementary Fig. 12c). We also directly compared the pc activity from a freely swimming and an immobilized larva on NeuBtracker to demonstrate that the same information could be obtained during tracking (Supplementary Fig. 12d).

The 2D galvanometric mirror system of NeuBtracker can also be used to project light patterns into the arena to provide, e.g., photostimulation. In order to demonstrate this feature, we coupled a 405-nm laser via the galvanometric mirrors and repeatedly steered the laser spot toward the head of the fish to elicit aversive responses at higher laser intensities (90-mW laser focused on a 200- $\mu$ m area) or contralateral tectal responses using lower laser power (Supplementary Fig. 13).

In summary, we introduced a modular and open-source neurobehavioral imaging system that enables simultaneous neuroimaging and behavioral monitoring of unrestrained, natural behaviors in different lines of zebrafish expressing calcium indicators. We took care to minimize uncontrolled stimulation of the animals by employing tracking via galvanometric mirrors and providing homogeneous illumination of the entire arena.

NeuBtracker may be augmented with concurrent multiplanar and volumetric detection (such as multifocus or light-field microscopy<sup>18</sup>), which could be combined with planar or patterned excitation techniques<sup>19</sup> for optical sectioning. In addition, coupling of lasers with the mirror-tracking system could enable focused illumination at defined coordinates to serve as visual stimuli or possibly trigger spectrally compatible optogenetic tools to eventually even obtain closed-loop control<sup>20</sup> of neuronal activity during neuroimaging of unrestrained behavior.

## METHODS

Methods, including statements of data availability and any associated accession codes and references, are available in the [online version of the paper](#).

*Note: Any Supplementary Information and Source Data files are available in the online version of the paper.*

## ACKNOWLEDGMENTS

We thank K. Kawakami and A. Muto (National Institute of Genetics (Japan)) for sharing *tg(gSA2AzGFF49A;UAS:GCaMP7a)* and *tg(gSA2AzGFF152B)*, here referred to as GR152:Gal4, which was provided to us by R. Portugues and L. Knogler (Max Planck Institute of Neurobiology), K. Asakawa (National Institute of Genetics (Japan)) for providing *tg(mnGFF7;UAS:eGFP)*, J. Ngai (University of California, Berkeley) for *tg(OMP4; UAS:GCaMP1.6)*,

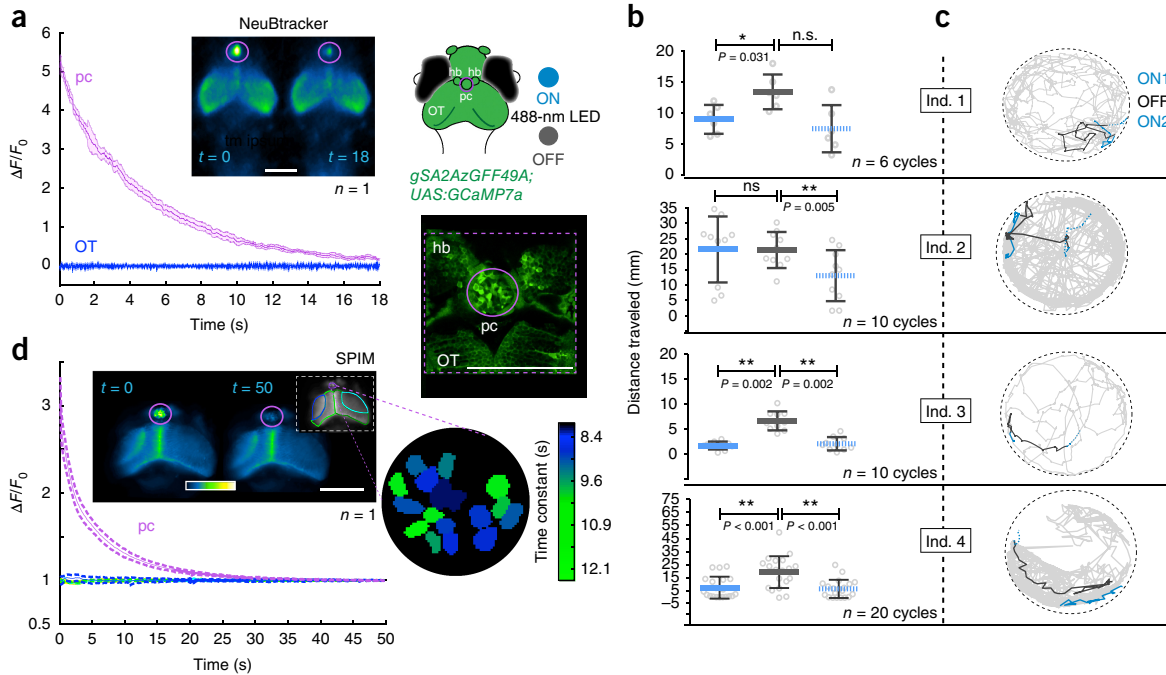


**Figure 3** | Neurobehavioral responses of the pineal complex (pc) to dark-light cycles in freely swimming larvae. **(a)** Fluorescence signal changes obtained with NeuTracker from pc and optic tectum (OT) in a larva expressing the calcium indicator GCaMP7a (*tg(gSA2AzGFF49A;UAS:GCaMP7a)*, 6 dpf). The signal was averaged over ten dark-light cycles and is plotted with s.e.m. Right, schematic drawing and two-photon microscopy image of the anterior larval zebrafish brain showing pc, habenulae (hb) and OT. The symbols indicate the color coding of the stimulation paradigm consisting of alternating periods of illumination with the LED ON (blue) or OFF (gray). **(b)** Plot of the median and the interquartile range of the locomotor activity (distance traveled) across different cycles (50 s light ON, 10 s OFF and 50 s ON again) for four individuals (*P* values were derived from a two-tailed Wilcoxon signed-rank test). **(c)** Plot of swimming trajectories color coded for the illumination condition for four animals. **(d)** Fluorescent signal time courses (averaged over three cycles, shown with s.e.m.) in pc (purple ROI) detected by SPIM in the same transgenic larvae immobilized in 1% low melting agarose. Additional signal trajectories are shown from ROIs in OT (color coding indicated in the inset). The zoom-in on the right shows a magnified view of pc with fitted time constant overlaid in color on top of the respective ROI. Scale bars, 200  $\mu\text{m}$  (a, d).

M. Ahrens (Janelia Research Campus) for sharing *tg(HuC:H2B-GCaMP6s)*, H. Baier and K. Slanec (Max Planck Institute of Neurobiology) for sharing *tg(HuC:Gal4;UAS:eGFP)* and *tg(HuC:Gal4;UAS:GCaMP6s)*, and L. Godinho (Technical University of Munich) for providing *tg(HuC:Gal4;UAS:GCaMP6s)*. We are grateful to J. Huisken and F. Fahrbach for providing assistance on building the SPIM; J. Fuchs assisted with the SPIM setup and experiment. We thank B. Wolfrum, P. Rinklin, J. Rebling, D. Razansky and the central machine shop of Helmholtz Zentrum Muenchen for help with the design and production of the arenas; H. Rolbieski for administrative support and help with data organization; T. Durovic and J. Ninkovic for assistance with the two-photon microscopy experiments; M. Fabiszak, C. Penningroth and L. Garrett for valuable comments on the manuscript. We are grateful for support from the European Research Council under grant agreements ERC-StG: 311552 (G.G.W., A.L., P.S.) and the Helmholtz Alliance ICEMED (G.G.W.).

#### AUTHOR CONTRIBUTIONS

P.S. designed and implemented NeuTracker with important contributions from H.J., M.K. and A.C.; programmed control software; conducted neurobehavioral imaging experiments including SPIM; analyzed data; and wrote the manuscript. A.L. designed and implemented neurobehavioral and two-photon experiments, conducted p-ERK imaging experiments, analyzed data, created illustrations and wrote the manuscript. A.S. and T.L. implemented image registration routines and improved tracking algorithm and analyzed data together with S.S. M.C. carried out the first implementation of tracking algorithm and performed original image and signal processing. C.C.P. carried out the initial implementation of SPIM. A.M. conducted photoaversion experiments on immobilized fish. A.S. was responsible for animal husbandry and provided support for neurobehavioral imaging. S.R. generated *tg(HuC:GCaMP6s)*. W.W. and V.N. supported the project and provided feedback on the manuscript. G.G.W. conceived and supervised the work, analyzed data and wrote the manuscript.

#### COMPETING FINANCIAL INTERESTS

The authors declare no competing financial interests.

Reprints and permissions information is available online at <http://www.nature.com/reprints/index.html>. Publisher's note: Springer Nature remains neutral with regard to jurisdictional claims in published maps and institutional affiliations.

- Kim, C.K. *et al. Nat. Methods* **13**, 325–328 (2016).
- Looger, L.L. & Griesbeck, O. *Curr. Opin. Neurobiol.* **22**, 18–23 (2012).
- Ahrens, M.B. & Engert, F. *Curr. Opin. Neurobiol.* **32**, 78–86 (2015).
- Portugues, R., Feierstein, C.E., Engert, F. & Orger, M.B. *Neuron* **81**, 1328–1343 (2014).
- Vladimirov, N. *et al. Nat. Methods* **11**, 883–884 (2014).
- Ahrens, M.B. *et al. Nature* **485**, 471–477 (2012).
- Muto, A., Ohkura, M., Abe, G., Nakai, J. & Kawakami, K. *Curr. Biol.* **23**, 307–311 (2013).
- Naumann, E.A., Kampff, A.R., Prober, D.A., Schier, A.F. & Engert, F. *Nat. Neurosci.* **13**, 513–520 (2010).
- Kalueff, A.V. *et al. Zebrafish* **10**, 70–86 (2013).
- Orger, M.B. & de Polavieja, G.G. *Annu. Rev. Neurosci.* **40**, 125–147 (2017).
- Bruni, G. *et al. Nat. Chem. Biol.* **12**, 559–566 (2016).
- Nguyen, J.P. *et al. Proc. Natl. Acad. Sci. USA* **113**, E1074–E1081 (2016).
- Grover, D., Katsuki, T. & Greenspan, R.J. *Nat. Methods* **13**, 569–572 (2016).
- Haesemeyer, M., Robson, D.N.N., Li, J.M.M., Schier, A.F.F. & Engert, F. *Cell Syst.* **1**, 338–348 (2015).
- Guggiana-Nilo, D.A. & Engert, F. *Front. Behav. Neurosci.* **10**, 160 (2016).
- Hussain, A. *et al. Proc. Natl. Acad. Sci. USA* **110**, 19579–19584 (2013).
- Randlett, O. *et al. Nat. Methods* **12**, 1039–1046 (2015).
- Prevedel, R. *et al. Nat. Methods* **11**, 727–730 (2014).
- Mertz, J. *Nat. Methods* **8**, 811–819 (2011).
- Grosenick, L., Marshel, J.H. & Deisseroth, K. *Neuron* **86**, 106–139 (2015).

## ONLINE METHODS

**Details on NeuTracker in MacroZoom configuration.** We exclusively used commercially available off-the-shelf components for construction of the open-source NeuTracker system (see the full list of components in **Supplementary Table 1** as well as schematics and photos of the design in **Supplementary Fig. 1**).

**Objective.** The FOV around the swimming arena (15 × 15 mm) was imaged by a 1× Nikon Objective from Stereo Microscope (HR Plan Apo WD 54).

**Illumination.** Excitation light was provided by a ~3.3 Watt LED (UHP-T-LED-460) coupled directly behind the objective using a dichroic (T495lpxr-UF1, Chroma) to illuminate the whole arena homogeneously and minimize thermal gradients that might have affected fish behavior<sup>14,15,21</sup>. A dichroic (T770lpxr, Chroma) was placed in a second filter cube to generate two images for the 1× and magnified paths; the relatively high residual transmission in the 530–560 nm range also allowed acquisition of both fluorescence and IR images from the low-magnification camera.

**1× detection.** The first image was projected by a 5:1 relay system (based on a pair of 150/30 mm achromatic doublets, Thorlabs) on the CCD of an IR-sensitive camera (MQ013RG-E2, Ximea), which was used for both the online tracking and behavioral recordings.

**Beam steering.** An *xy*-galvanometric mirror pair (GVS312/M, Thorlabs) was placed between a scan lens (constructed using a Plössl-type configuration with two 100 mm achromatic doublets placed back to back (effective focal length, 50 mm) and a tube lens (achromatic doublet  $f = 150$ , Thorlabs)). This ensemble projects the region of interest in the center of the FOV of a zoom lens system. The mirrors can be both moved manually and driven by the automatic tracking routine (see below).

**Tunable lens.** Close to the intermediate focus point of the scanning lens, an electrically focus-tunable lens (EL-10-30, Optotune) was placed to enable focusing at different *z*-planes.

**Magnifications.** The centered and focused images were captured by a zoom lens system (Z16, Leica with a 0.5× Objective), which enabled variable magnification in the range of 0.5× to 15×.

**Fluorescence detection.** A scientific CMOS (sCMOS) camera (Zyla5.5, Andor) was used to capture the fluorescence signals through an ET525/50m (Chroma) emission filter with exposure times as short as 5 ms. The sensitivity of the camera is also sufficient for using a fluorescent plastic slide (Chroma) as a light source and capturing transillumination imaging at >50 FPS (**Supplementary Fig. 2**), which enables high-resolution behavioral and anatomical imaging.

**Details on NeuTracker in MicroFixed configuration.** To evaluate the modularity of the imaging platform, a second version of NeuTracker ('MicroFixed') was assembled in which a series of modifications were tested. A Nikon 1× Microscopy Objective lens (CFI P-Achromat UW 1×/0.04/3.20) and a 200 mm tube lens (ITL 200 Thorlabs) were used to form the first images using the same LED source as in the 'MacroZoom' configuration that was coupled in the infinity space between the lenses. Infrared illumination (IR) was provided by a ring housing 12 LEDs (ELD-1060-525) centered at 1,060 nm, a wavelength that is invisible to the fish<sup>22</sup>, and the beam splitter was replaced by a dichroic mirror (T770lpxr,

Chroma). The single 30 mm achromatic doublet worked both as a scanning lens and as the first lens of a 4-f Keplerian telescope. The modified 4-f system between the scan lens and the tube lens (200 mm in this version) also served as a magnifier and resulted in an ~7× magnification (200/30 = 6.6). Based on this configuration of the platform, a series of add-ons were tested, including the coupling of a 405 nm laser for tracked photostimulation and an *x*-stage for screening multiwell plates. The use of the microscope objective and a fixed magnification resulted in an overall lower sensitivity and resolution, a slightly smaller FOV (10 × 10 mm), and a more restricted working distance (1 cm). Nonetheless, the imaging data delivered comparable biological information in direct comparison to the MacroZoom configuration (**Fig. 3a** and **Supplementary Fig. 13a**).

### Acquisition control software and automation of experimental procedures.

A modular architecture based on Matlab (v.2014-2016, Mathworks) was used to ensure compatibility with various cameras, galvanometric mirrors and other controllable items (ETL, stimulation devices) while enabling fast prototyping with easy additions of pre-existing or custom-built routines in the acquisition pipeline. Two graphic user interfaces (GUIs) controlled five additional Matlab workers (W1-5), which were running asynchronously on a single PC (i7-3770, 32GB RAM) exchanging most recent data using a RAM-disk (**Supplementary Fig. 4**; open-source code available as **Supplementary Software** and on <http://www.neubtracker.org>).

**Graphical user interface 1 'control panel'.** Apart from the initialization of the system, GUI1 provides overall system control ('start/stop, tracking/recording'), panels for previewing intermediate results (e.g., 'tracking input') and other options for manually inserting comments on the whole experiment and/or current timepoint.

**Graphical user interface 2, 'the previewer'.** GUI2 shows the most recent 1× and fluorescence images with sliders enabling window/level. The same GUI is also used to preview tracking output and the *xy*-location of the galvanometric mirrors and enables the 'click-to-aim' manual tracking override by clicking on the desired target position in the whole FOV image. The same panel can also be used for viewing previously acquired data sets (in their raw form).

**W1 and 2 camera control.** These workers acquire continuously from the 1× IR-sensitive and the fluorescence channel and save the data along with metadata to a disk in binary format.

**W3 tracking and aiming.** W3 detects the center of mass of the fish from the IR channel. Once the coordinates are determined, they are transformed (based on a fixed transformation matrix built during a calibration step) into a pair of voltage values. If the center of mass exceeds a predefined distance from the center of FOV, these voltage command signals are sent via an IO card (NI USB-9263) to the galvanometric mirrors that move the FOV of the fluorescent channel (**Supplementary Figs. 4–6**). Manual overrides of the automated tracking are possible by either defining the desired coordinates of the FOV via a mouse click or by moving the FOV with a joystick.

**W4 autofocus.** This worker calculates a focus measure (Brenner's method provided the best trade-off between speed and robustness from different methods tested<sup>23</sup>) and if necessary adjusts the focal length of the ETL by acquiring a few images in adjacent focal planes

and fitting a second-degree polynomial to estimate the optimal focus (**Supplementary Fig. 8**).

**W5 data logistics.** this worker is responsible for cleaning the acquisition folder on the RAM-Disk by deleting not-recorded images (of the preview phases or between experiments) and archiving recorder frames during long acquisitions.

The Matlab-based acquisition framework enables the control of additional devices from the main platform (e.g., initializing stimulation schedules via an Arduino Microcontroller, Psytoolbox streaming to a projector positioned under the sample, control of translational stages for moving between samples located in multiwell arenas). The GUI allows for saving metadata during the experiment indexed to specific timepoints.

**Data processing pipeline.** Each single output data set of NeuBTracker is composed of two collections of images: one acquired by the fluorescence channel and one obtained from the 1× channel. This section describes the process of data analysis of the fluorescence images.

**Quality check.** An automated quality inspection of the fluorescence images (**Supplementary Fig. 4** and **Supplementary Video 1**) is performed in two stages. In the first stage, a fast and robust feature detection algorithm (SURF) is run on each single frame. The number of features detected is the first parameter considered in order to confirm the presence of the brain in the FOV in each frame. Any frame with less than five features detected is censored from subsequent analyses. In the second stage, the individual frames are grouped into batches. In each batch, an image with a high number of features is selected as a key frame, which is a good indicator for the presence of the brain in the FOV. All other frames in the batch are matched to the key frame using a similarity transform. Frames that yield no match to the key frame are censored, as well as frames that have a similarity transform with nonunit scaling (thresholded at  $\pm 0.1$ ). The transformed frames in the batches are used as initialization for the subsequent registration routine.

**Registration.** To initialize the registration process, the key frame in each batch and the estimated transform computed from the feature matching (see quality check) are used. The frames in each batch are then cropped around the estimated position of the fish (see quality check) to reduce the file size. The registration then proceeds in three steps. First, for each batch the frames are registered to the key frame using an intensity-based registration algorithm maximizing the mutual information similarity measure, applying a rigid transformation model (see **Supplementary Figs. 4** and **7**; **Supplementary Video 1**). In a second step, a global template image is selected from the key frames. All frames of the image series are then rigidly registered to the global template by applying the same registration algorithm again, propagating the previous transformations. As a final step for fine tuning the registration result, all frames are again registered with respect to the global template. This is performed by optimizing the cross-correlation of the images in the Fourier domain and applying a transformation model using only translations.

**Signal analysis.** Fluorescence signals were normalized using different estimates of low-frequency trends as indicated in each figure legend.

**Transgenic lines for neurobehavioral experiments.** All animal experiments were conducted in accordance with the guidelines

approved by the government of Upper Bavaria. 24 h embryos were collected from the parents and reared with a 14:10 light:dark cycle according to a standard protocol at 28 °C<sup>24</sup>. Positive fish expressing calcium indicators (tg(*gSA2AzGFF49A*;UAS:*GCaMP7a*)<sup>7</sup>, tg(*HuC:GCaMP6s*), tg(*HuC:H2BGCaMP6s*), tg(*gSA2AzGFF152B*;UAS:*GCaMP6s*)<sup>25,26</sup> herein referred to as *GR152:Gal4*) and GFP controls tg(*HuC:Gal4*;UAS:*eGFP*) and tg(*OMP4*;UAS:*GCaMP1.6*;mn*GFF7*:GFP)<sup>27</sup>, were selected between 72–96 hpf. The tg(*HuC:Gal4*;UAS:*eGFP*) were treated with PTU (N-Phenylthiourea  $\geq 98\%$ , Sigma-Aldrich) to inhibit melanin production. Imaging on NeuBTracker is noninvasive, and animals can be reimaged at different timepoints with NeuBTracker, SPIM or confocal microscopy.

**Test arenas.** We used NeuBTracker with a FOV of 15 × 15 mm and a working distance between objective and sample of ~10 cm. Any plastic dish (e.g., P35G-007-C, MATEK) with transparent bottom, heights of 2 mm–1 cm and a diameter <1.5 cm can be used as an arena. To enable long-term recordings and controlled application of substances (e.g., odors), we designed custom-made circular arenas of 9 mm in diameter (see **Supplementary Fig. 10**) that contain two symmetric holes <10 μm connected to two ~25 μL compartments into which substances can be directly pipetted via external injection ports. We observed that a syringe pump running at 0.3 mL/h was able to adequately compensate water evaporation during experiments lasting more than 1 h. To ensure minimal contamination between experiments, the bottom of the custom-made arenas consists of a glass coverslip that can be changed between experiments. Versions with separators in the middle of the arena can be used either to generate local gradients of compounds injected through the ports or to enforce more complex swimming trajectories. Those designs can be implemented by CNC milling using different materials (such as anodized aluminum, which was used in the experiments with cadaverine). The addition of an *xy*-stage with a 3D printed coverslip holder enables the use of multiwell plates, while the large working distance provides enough space for future automation<sup>28</sup>.

**Pharmacological neurostimulation experiments.** After 10 s of acclimation, larvae tg(*HuC:GCaMP6s*) (5 dpf) were imaged at a baseline while freely exploring the NeuBTracker arena before 10 μL of a 1,200 μM 4-AP solution (4-Aminopyridine, Sigma-Aldrich) was added at 150 s (t1) to one group of fish, while another group received only fish water at 150 s and 10 μL of 1,200 μM 4-AP at 300 s (t2). The exact injection timepoints were recorded on the 1× camera to temporally align each experimental run. Fish were randomly assigned to the experimental groups; data were processed with knowledge of the group assignment (no blinding).

**Photostimulation experiments.** Single zebrafish larvae tg(*gSA2AzGFF49A*; UAS:*GCaMP7a*) (6 dpf) were left free to explore a circular arena (9 mm) on NeuBTracker (containing ~100 μL of fish water). After a few seconds of acclimation, an automated tracker control routine was initiated that switched the 488 nm LED illumination OFF and ON (5 s OFF and 20 s ON (**Fig. 3a**) or 10 s OFF and 50 s ON (**Supplementary Fig. 13a**)) for several cycles to test for responses of the pineal complex known to contain photoreceptors<sup>29</sup>. Sample sizes were chosen based on preliminary experiments that showed robust activations of the

pineal complex in this stimulation paradigm. As the dynamics of neuronal activation in response to the OFF–ON were studied within each subject, no randomized assignment to experimental groups was made; data processing was performed with knowledge of the stimulation schedule (no blinding). For validation experiments, a custom-built single-plane illumination (SPIM) setup was used, which combines both a fast galvo-scanner light sheet<sup>30</sup> and an ETL<sup>31</sup> for the *z*-scanning of the optical path. The larvae were embedded in 1% low melting agarose in a custom-made chamber and illuminated by a light sheet (~10 μm thick) generated by a 488 nm laser (Obis, Coherent). One plane was imaged at 10 Hz. The same OFF–ON sequence used with NeuBtracker was applied for the stimulation using a beam blocker. Activation of the pineal complex was confirmed by immunodetection of phosphorylated ERK<sup>17</sup> on a different group of larvae of the same age and strain using the same dark–light cycles protocol as was used for the NeuBtracker (pERK antibody (Cell Signaling, 4370) and tERK antibody (Cell Signaling, 4696) with secondary anti-mouse AF 488 AB from Abcam ab150113 and anti-rabbit DyLight 594 from ThermoFisher Scientific, Cat # 35560).

**Statistical analysis. Spontaneous swimming.** To obtain the statistical map shown in **Figure 1c**, a linear regression between the relative change in the fluorescence signal and the swimming speed was computed for each voxel and coefficients displayed for *P* values < 10<sup>-5</sup> (corresponds to *P* < 0.01, Bonferroni corrected for 1,000 voxels, two-sided *t*-test on the linear regression coefficient). For the scatter plots in **Supplementary Figure 9**, we used the same model on the signal time courses averaged over the indicated ROIs. For cluster analysis (**Supplementary Fig. 9**), the time trace for each pixel in the image was transformed using a principal component analysis, followed by fitting a Gaussian Mixture Model (GMM) with Expectation Maximization (EM) on the first 100 components explaining more than 90% of the variance.

**Olfactory stimulation with cadaverine.** The representative result shown in **Figure 1e** is complemented with control experiments shown in **Supplementary Figure 11**. The behavioral analysis was conducted by EthoVision XT software and custom-written Matlab routines and statistics were computed in GraphPad Prism 6 (two-tailed Wilcoxon matched-pairs signed rank test, *n* = 8 with *P* values for the different metrics reported in the legend of **Supplementary Fig. 11d**).

**Pharmacological stimulation with 4-AP.** Differences in fluorescent signal changes as well as differences in swimming speed (shown with s.e.m. between and within experimental groups) were analyzed with unpaired or paired *t*-tests respectively, *n* = 4, with *P* values for the different comparisons indicated in the legend of **Fig. 2**.

**Photostimulation of pc.** The fluorescent signal time courses are shown averaged over ten cycles in one animal (**Fig. 3a,e**, with s.e.m.) or over four animals (**Supplementary Fig. 12a**). Control experiments are shown in **Figure 12b–d**. The corresponding behavioral data in **Figure 3c** were analyzed for each animal by a two-tailed Wilcoxon signed-rank test with the *P* values for each individual indicated in the figure legend.

**Code availability.** Additional detailed documentation of the optomechanical design along with assembly files, 3D files of the arena and the complete Matlab code (under a creative commons license) for automation and analysis can be found at <http://www.neubtracker.org/>.

**Data availability statement.** The data supporting the findings of this study are available from the corresponding author upon reasonable request.

A summary of the experimental design, statistical parameters and zebrafish lines used in this study can be found in the **Life Sciences Reporting Summary**.

- Chen, X. & Engert, F. *Front. Syst. Neurosci.* **8**, 39 (2014).
- Shcherbakov, D. *et al. PLoS One* **8**, e64429 (2013).
- Pertuz, S., Puig, D. & Garcia, M.A. *Pattern Recognit.* **46**, 1415–1432 (2013).
- Kimmel, C.B., Ballard, W.W., Kimmel, S.R., Ullmann, B. & Schilling, T.F. *Dev. Dyn.* **203**, 253–310 (1995).
- Takeuchi, M. *et al. Dev. Biol.* **397**, 1–17 (2015).
- Knogler, L.D., Markov, D.A., Dragomir, E.I., Štíh, V. & Portugues, R. *Curr. Biol.* **27**, 1288–1302 (2017).
- DeMaria, S. *et al. J. Neurosci.* **33**, 15235–15247 (2013).
- Pardo-Martin, C. *et al. Nat. Methods* **7**, 634–636 (2010).
- Li, X. *et al. PLoS One* **7**, e40508 (2012).
- Keller, P.J., Schmidt, A.D., Wittbrodt, J. & Stelzer, E.H.K. *Science* **322**, 1065–1069 (2008).
- Fahrbach, F.O., Voigt, F.F., Schmid, B., Helmchen, F. & Huisken, J. *Opt. Express* **21**, 21010–21026 (2013).

## Life Sciences Reporting Summary

Nature Research wishes to improve the reproducibility of the work that we publish. This form is intended for publication with all accepted life science papers and provides structure for consistency and transparency in reporting. Every life science submission will use this form; some list items might not apply to an individual manuscript, but all fields must be completed for clarity.

For further information on the points included in this form, see [Reporting Life Sciences Research](#). For further information on Nature Research policies, including our [data availability policy](#), see [Authors & Referees](#) and the [Editorial Policy Checklist](#).

### Experimental design

1. Sample size

Describe how sample size was determined.

The sample size was estimated from reported literature and pilot experiments.

2. Data exclusions

Describe any data exclusions.

Imaging frames of insufficient quality (based on the algorithm and criteria presented in the text and in Supplementary Figures 4,6,7) were excluded from subsequent analyses.

3. Replication

Describe whether the experimental findings were reliably reproduced.

Experimental findings were replicated several times in different animals and for most experiments also across different imaging conditions.

4. Randomization

Describe how samples/organisms/participants were allocated into experimental groups.

In each experiment the larvae for each group (e.g. late vs. early delivery of 4-AP) were selected randomly from the same population. When different lines (e.g. GFP) were used as controls, those were mated on the same date and grown up under identical conditions.

5. Blinding

Describe whether the investigators were blinded to group allocation during data collection and/or analysis.

No blinding of investigators to group allocation took place but the data acquisition and analysis pipeline was identical for all experimental groups and the analyses did not involve human scoring.

Note: all studies involving animals and/or human research participants must disclose whether blinding and randomization were used.

6. Statistical parameters

For all figures and tables that use statistical methods, confirm that the following items are present in relevant figure legends (or in the Methods section if additional space is needed).

n/a Confirmed

- The exact sample size ( $n$ ) for each experimental group/condition, given as a discrete number and unit of measurement (animals, litters, cultures, etc.)
- A description of how samples were collected, noting whether measurements were taken from distinct samples or whether the same sample was measured repeatedly
- A statement indicating how many times each experiment was replicated
- The statistical test(s) used and whether they are one- or two-sided (note: only common tests should be described solely by name; more complex techniques should be described in the Methods section)
- A description of any assumptions or corrections, such as an adjustment for multiple comparisons
- The test results (e.g.  $P$  values) given as exact values whenever possible and with confidence intervals noted
- A clear description of statistics including central tendency (e.g. median, mean) and variation (e.g. standard deviation, interquartile range)
- Clearly defined error bars

See the web collection on [statistics for biologists](#) for further resources and guidance.



## ► Software

Policy information about [availability of computer code](#)

### 7. Software

Describe the software used to analyze the data in this study.

We used custom routines written in Matlab which are available in the zip file provided as Supplementary Information on NeuBTracker.org. For preliminary visualization of the data, Fiji was used (Schindelin, J.; Arganda-Carreras, I. & Frise, E. et al. (2012), "Fiji: an open-source platform for biological-image analysis", Nature methods 9(7): 676-682, PMID 22743772) as well as AFNI (Cox, R. W. AFNI: software for analysis and visualization of functional magnetic resonance neuroimages. Comput. Biomed. Res. 29, 162–173 (1996).)

For manuscripts utilizing custom algorithms or software that are central to the paper but not yet described in the published literature, software must be made available to editors and reviewers upon request. We strongly encourage code deposition in a community repository (e.g. GitHub). *Nature Methods* [guidance for providing algorithms and software for publication](#) provides further information on this topic.

## ► Materials and reagents

Policy information about [availability of materials](#)

### 8. Materials availability

Indicate whether there are restrictions on availability of unique materials or if these materials are only available for distribution by a for-profit company.

-

### 9. Antibodies

Describe the antibodies used and how they were validated for use in the system under study (i.e. assay and species).

-

### 10. Eukaryotic cell lines

a. State the source of each eukaryotic cell line used.

-

b. Describe the method of cell line authentication used.

-

c. Report whether the cell lines were tested for mycoplasma contamination.

-

d. If any of the cell lines used are listed in the database of commonly misidentified cell lines maintained by [ICLAC](#), provide a scientific rationale for their use.

-

## ► Animals and human research participants

Policy information about [studies involving animals](#); when reporting animal research, follow the [ARRIVE guidelines](#)

### 11. Description of research animals

Provide details on animals and/or animal-derived materials used in the study.

tg(HuC:GCaMP6s)  
 tg(HuC:H2B-GCaMP6s)  
 tg(GR152:Gal4;UAS:GCaMP6s) [tg(gSA2AzGFF152B) referred to as GR152:Gal4]  
 tg(gSA2AzGFF49A;UAS:GCaMP7a)

tg(OMP4; GCaMP1.6 x mnGFF7; UAS:eGFP)  
 tg(HuC:Gal4;UAS:GCaMP6s)  
 tg(HuC:Gal4;UAS:eGFP)

Policy information about [studies involving human research participants](#)

### 12. Description of human research participants

Describe the covariate-relevant population characteristics of the human research participants.

-